Smart Structures and Systems, *Vol. 31, No. 5 (2023) 437-454*
https://doi.org/10.12989/sss.2023.31.5.437

A model-based adaptive control method for real-time hybrid simulation

Xizhan Ning [1,2a], Wei Huang [1b], Guoshan Xu[*3,4,5], Zhen Wang [6c] and Lichang Zheng [3d]

[1] *College of Civil Engineering, Huaqiao University, Xiamen 361021, China*
[2] *Key Laboratory for Intelligent Infrastructure and Monitoring of Fujian Province, Huaqiao University, Xiamen 361021, China*
[3] *School of Civil Engineering, Harbin Institute of Technology, Harbin 150090, China*
[4] *Key Lab of Structures Dynamic Behavior and Control, Ministry of Education, Harbin Institute of Technology, Harbin 150090, China*
[5] *Key Lab of Intelligent Disaster Mitigation, Ministry of Industry and Information Technology, Harbin 150090, China*
[6] *School of Civil Engineering and Architecture, Wuhan University of Technology, Wuhan 430070, China*

(*Received July 22, 2022, Revised December 29, 2022, Accepted March 3, 2023*)

Abstract. Real-time hybrid simulation (RTHS), which has the advantages of a substructure pseudo-dynamic test, is widely used to investigate the rate-dependent mechanical response of structures under earthquake excitation. However, time delay in RTHS can cause inaccurate results and experimental instabilities. Thus, this study proposes a model-based adaptive control strategy using a Kalman filter (KF) to minimize the time delay and improve RTHS stability and accuracy. In this method, the adaptive control strategy consists of three parts—a feedforward controller based on the discrete inverse model of a servo-hydraulic actuator and physical specimen, a parameter estimator using the KF, and a feedback controller. The KF with the feedforward controller can significantly reduce the variable time delay due to its fast convergence and high sensitivity to the error between the desired displacement and the measured one. The feedback control can remedy the residual time delay and minimize the method's dependence on the inverse model, thereby improving the robustness of the proposed control method. The tracking performance and parametric studies are conducted using the benchmark problem in RTHS. The results reveal that better tracking performance can be obtained, and the KF's initial settings have limited influence on the proposed strategy. Virtual RTHSs are conducted with linear and nonlinear physical substructures, respectively, and the results indicate brilliant tracking performance and superb robustness of the proposed method.

Keywords: benchmark; Kalman filter; model-based adaptive control; real-time hybrid simulation; time delay

1. Introduction

Hybrid simulation (HS), also known as substructure pseudo-dynamic test (Hakuno *et al*. 1969), is an advanced seismic test method that can reproduce the structural response under earthquake excitation (Nakashima 2020). In HS, the target structure is typically divided into the numerically simulated part (called numerical substructure, NS) and the physically tested part (called physical substructure, PS), which can greatly decrease the size and scale of the specimen, and then overcome practical problems caused by test location and costs (Qian *et al*. 2014). However, the HS cannot evaluate the seismic capacity of velocity-related specimens or structures due to a decrease in the loading speed (Blakeborough *et al*. 2001). Thus, Nakashima *et al*. (1992) proposed a real-time hybrid simulation (RTHS) to address the aforementioned problem, where the boundary condition between the NS and PS must be completed accurately in real-time over a tiny time span (Drazin and Govindjee 2017, Chen and Chen 2020, Najafi and Spencer 2021). According to the control mode, RTHS can be divided into force- (Shao and Reinhorn 2012) and displacement-based RTHS (Chen *et al*. 2022), and this study focuses on the latter. It is worth noting that de-synchronization between the two substructures emerges, mainly caused by the dynamic characteristics of loading systems. This phenomenon is typically called time delay, which brings challenges to the accuracy and stability of RTHS (Wallace *et al*. 2005). Hence, time delay needs to be effectively compensated for using a suitable control method.

Time delay compensation methods can be roughly divided into three categories: invariant delay-based, control theory-based, and adaptive time delay control methods. The first category mainly includes polynomial extrapolation (Horiuchi *et al*. 1999) and its improvement, kinematic predict method (Horiuchi and Konno 2001), and they cannot effectively deal with the varying time delay problem in RTHS. The second is the control theory-based methods, which can be further divided into classical and modern control theory-based methods. In the former methods, loading devices and specimens, which are considered the control plant, can be expressed by a transfer function, and the time delay is compensated for using the inverse control method (Chen and Ricles 2009), feedforward–feedback control method (Phillips and Spencer 2013), model-based

*Corresponding author, Associate Professor,
E-mail: xuguoshan@hit.edu.cn
[a] Associate Professor, E-mail: xzning@hqu.edu.cn
[b] Graduate Student, E-mail: huang_wei1996@163.com
[c] Professor, E-mail: wang_zhen@whut.edu.cn
[d] Graduate Student, E-mail: 19s133151@hit.edu.cn

ISSN: 1738-1584 (Print), 1738-1991 (Online)

control method (Carrion and Spencer 2007, 2008, Zhou and Li 2021), phase-lead control (Zhao *et al*. 2003), and so on. The latter mainly includes slide mode control method (Li *et al*. 2021), H_∞ control method (Gao *et al*. 2013, Ning *et al*. 2019), and RLQG (Zhou *et al*. 2019). Third, adaptive time-delay control methods, which integrate system identification or parametric estimation, have piqued significant interest in recent years. The adaptive control law is constructed by inverse control (Chen and Ricles 2010, Chen *et al*. 2012), adaptive time series (Chae *et al*. 2013), adaptive forward prediction (Marsico 2014), adaptive method utilizing online delay estimation (Wang *et al*. 2014), model-based control (Chen *et al*. 2015, Najafi and Spencer 2019, Gálmez and Fermandois 2022), and the discrete model of the control plant (Ning *et al*. 2022, Wang *et al*. 2020).

To handle the variable time delay in RTHS more efficiently, adaptive control methods based on nonlinear control theories have been drawn considerable attention in recent years, such as passivity adaptive control based on the energy flow in RTHS (Peiris *et al*. 2021), backstepping control derived by Lyapunov stability analysis (Ouyang *et al*. 2019), and adaptive slide mode control (Li *et al*. 2022). In addition, adaptive strategies combining different control theories have been proposed and exhibit high control accuracy. For instance, Tao and Mercan (2019) proposed a tracking error-based adaptive method, along with a proportional-integral-derivative controller; Xu *et al*. (2019) proposed an adaptive controller, which integrated the slide mode control and improved adaptive polynomial-based forward prediction; Wang *et al*. (2019) proposed the adaptive two-stage delay control strategy, which combines the adaptive controller and polynomial extrapolation. Those methods all exhibit outstanding tracking ability by virtual RTHSs or actual experiment investigations.

Generally, parameter estimation plays an important role in most adaptive control strategies. A parameter estimation method with excellent ability is mainly represented by three aspects: (i) the guarantee of convergence; (ii) low dependency for the initial parameter setting; (iii) high sensitivity to errors between the desired displacement and measured one. Among the parameter estimation methods, the Kalman filter (KF) exhibits a satisfactory performance. Ning *et al*. (2020) proposed an adaptive compensator based on KF, termed as KF-ADC, and then numerically validated using the RTHS Benchmark problem. However, there are two user-defined parameters determined by the control plant order, which can seriously affect the performance of KF-ADC. Moreover, the robustness of KF-ADC, essentially a feedforward controller, may be severely decreased when considering the disturbances in RTHS, such as the nonlinearity of PS.

This study aims to develop a user-friendly adaptive control strategy. Under the framework of feedforward and feedback control, a model-based adaptive control strategy using a Kalman filter (MAC-KF) is proposed to address the variable time delay problems. The proposed control strategy consists of three parts—a feedforward controller based on a discrete inverse model of the control plant, a parameter estimator using the KF algorithm, and a feedback controller. The main sections of this study are as follows. Section 2 briefly describes the problem statement in RTHS. Then, Section 3 presents a model-based adaptive control strategy using KF, i.e., MAC-KF. The reference structure and benchmark problem are given in Section 4, where the controllers are designed and verified. Subsequently, Section 5 investigates the parametric analysis of the proposed control strategy. Finally, Section 6 presents the RTHS results in benchmark problems with the linear and nonlinear PSs.

2. Problem statement

In RTHS or HS, the target structure is generally split into two types of substructures—the numerical substructure (NS) and the physical substructure (PS). The PS is the part with complex nonlinearity, whose mechanical properties cannot be well expressed analytically, and is tested in the laboratory. The NS is numerically simulated by a computer program. The equation of the motion (EOM) of the NS can be written as follows

$$\mathbf{M}_N\ddot{\mathbf{x}}_N+\mathbf{C}_N\dot{\mathbf{x}}_N+\mathbf{K}_N\mathbf{x}_N+\mathbf{f}_P(\mathbf{x}_P, \dot{\mathbf{x}}_P, \ddot{\mathbf{x}}_P) = -\mathbf{M}_N\boldsymbol{\theta}\ddot{x}_g \quad (1)$$

where $\mathbf{M}_N$, $\mathbf{C}_N$, and $\mathbf{K}_N$ are the matrix, damping, and stiffness matrixes of the NS, respectively; $\mathbf{x}$, $\dot{\mathbf{x}}$, and $\ddot{\mathbf{x}}$ are the displacement, velocity, and acceleration vectors of the structure, respectively; the subscripts N and P denote the NS and PS, respectively; $\mathbf{f}_P$ is the restoring force vector obtained directly from the experimental data; $\boldsymbol{\theta} = \{\mathbf{1}\}_{m\times 1}$, where m is the number of the degrees of freedom; $\ddot{x}_g$ denotes the seismic excitation.

Fig. 1 demonstrates the typical flowchart of RTHS with displacement control, mainly including three procedures. Eq. (1) is solved first by a proper numerical integration method. Then, the displacement, $\mathbf{x}_P$, calculated by the EOM is imposed on the PS by the loading systems, such as an actuator or shaking table. Finally, the restoring force, $\mathbf{f}_P$, measured from the PS is fed back to the NS. These procedures are repeated until the end of the earthquake excitation record.

In ideal RTHS, the boundary conditions between the two substructures must be satisfied, that is, the $\mathbf{x}_P$ is equal to the $\mathbf{x}_N$. However, owing to the dynamics of the loading system, its displacement response cannot be fully realized,

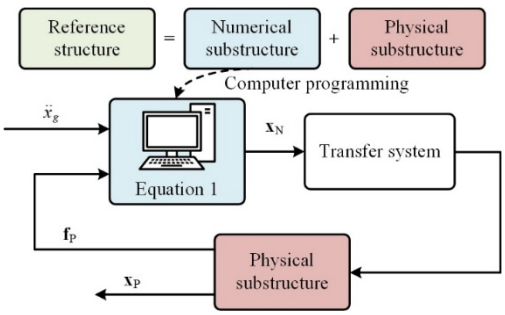

Fig. 1 Typical flowchart of RTHS

resulting in the de-synchronization of boundary conditions. In addition, the de-synchronization also is caused by the signal transition, experimental noise, nonlinearities of the PS and its interaction with the loading system. This de-synchronization phenomenon is often known as time delay. Due to the existence of time delay, experimental errors aroused, which will not only reduce the accuracy but also seriously affect the stability of RTHS. Moreover, it is studied that the time delay is not a constant value (Darby *et al*. 2002), it varies with both the frequency of excitation and specimen conditions (Phillips and Spencer 2013, Huang *et al*. 2019). Therefore, it is an effective approach to adopt adaptive compensation methods or control strategies to eliminate the time delay.

3. Model-based adaptive control strategy using Kalman filter

Fig. 2 shows the block diaphragm of the proposed adaptive control strategy, MAC-KF. It is seen in the figure, the proposed control method comprises three modules—a feedforward controller, a parameter estimator using KF, and a feedback controller. The feedforward controller is designed utilizing the discrete inverse model of the control plant, it can compensate for the control plant's time delay and reduce the amplitude error between the desired displacement d and the measured displacement d_{m}. The estimator estimates the parameters of the control plant using the relationship of displacement command and measurement in real-time. The feedback controller can further decrease the time delay and improve the robustness of the controlled system. The reason for using the discrete inverse model in MAC-KF is to facilitate implementation on digital signal processing boards and online identification of the control plant.

3.1 Parameterized feedforward controller based on the discrete inverse model

In general, the control plant can be represented by a rational proper transfer function from the commanded displacement d_{c} to the measured displacement d_{m}, as follows

$$G_s(s) = \frac{N_0}{D_n s^n + D_{n-1} s^{n-1} + \ldots + D_1 s + D_0} \tag{2}$$

where s is the Laplace operator, n and N_0 denote the order number and the gain of the transfer function, respectively, and $D_n, D_{n-1}, \ldots, D_0$ represent the coefficients of the denominator. To eliminate the time delay, the inverse model of the control plant can be served as a feedforward controller, which can be expressed as follows

$$\begin{aligned} G_{\mathrm{FF}}(s) &= \frac{D_n s^n + D_{n-1} s^{n-1} + \ldots + D_1 s + D_0}{N_0} \\ &= a_n s^n + a_{n-1} s^{n-1} + \ldots + a_1 s + a_0 \end{aligned} \tag{3}$$

where $a_0, \ldots, a_n$ denote the parameters of the feedforward controller. However, Eq. (3) is not a rational proper function and has no practical significance in control theory. However, considering the transformation between the Laplace domain and the time domain, the compensated displacement can be expressed in the time domain as follows

$$d_{\mathrm{c}}^{\mathrm{FF}} = a_n d^{(n)} + a_{n-1} d^{(n-1)} + \ldots + a_1 \dot{d} + a_0 d \tag{4}$$

where $d_{\mathrm{c}}^{\mathrm{FF}}$ is the displacement generated by the feedforward controller, d is the desired displacement, and the superscript (n) represents the n-degree derivative of the desired displacement. However, the responses obtained by Eq. (2) often differ from the actual ones, causing the controller not to function as expected, because the parameters in Eq. (4) originated from the transfer function (namely, Eq. (2)). One solution is to identify the control plant's transfer function and calculate the parameters $a_0, \ldots, a_n$ in real time. However, this procedure is extremely complicated. An alternative way is to introduce a differential equation into Eq. (4), which results in the following equation

$$d_{\mathrm{c},k}^{\mathrm{FF}} = x_{1,k} d_k + x_{2,k} d_{k-1} + \ldots + x_{n+1,k} d_{k-n} = \sum_{j=0}^{n} x_{j+1,k} d_{k-j} \tag{5}$$

where $x_1, x_2, \ldots, x_{n+1}$ are control plant parameters (CPPs) that relate to the parameters $a_0, \ldots, a_n$ and the sample time Δt in a discrete system; k is the k^{th} time step. Intrinsically, Eq. (5) represents the control plant's inverse model in the discrete-time domain, making it possible to estimate the CPPs using the commanded and measured displacements. Thus, a parameterized feedforward controller can be obtained.

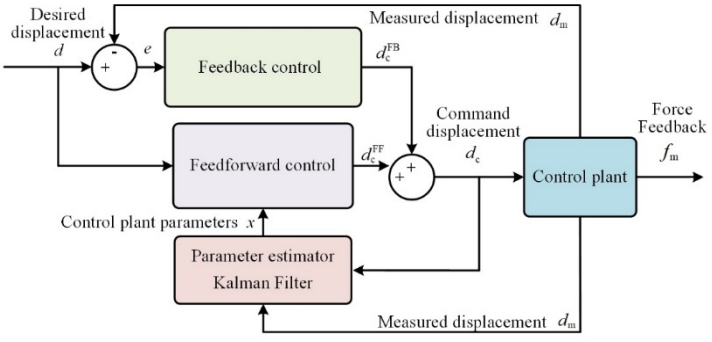

Fig. 2 Diaphragm of model-based adaptive control strategy using Kalman filter

3.2 Parameter estimation using Kalman filter

As shown in Fig. 2 and stated above, the parameter estimation method plays an important role in ensuring the excellent performance of the feedforward controller. Therefore, efficient and stabilized parameter estimation methods are more attractive. The least-squares method with the forgetting factor has attracted significant attention in the past since the CPPs are derived from the transfer function, which represents a linear relationship between input and output. However, the forgetting factor has a significant impact on the estimated parameters, which will affect the performance of the feedforward controller. Research showed that the KF exhibits excellent performance in linear estimation. Hence, the KF algorithm is used to estimate the control plant's parameters in this study. The state-space equations of the parameter estimation problem can be expressed as follows

$$\mathbf{x}_{k+1} = \mathbf{x}_k \tag{6}$$

$$z_k = \mathbf{H}_k \mathbf{x}_k + v_k \tag{7}$$

where $\mathbf{H}_k = \left[d_{\mathrm{m},k}, d_{\mathrm{m},k\text{-}1}, \ldots, d_{\mathrm{m},k\text{-}\mathrm{n}}\right]$, $d_{\mathrm{m},k}$ and z_k are the measured displacement and the command one at the k-th step, and v is the measurement noise that satisfies the following

$$\mathbf{E}v_k = 0, \mathbf{E}(v_k v_k^{\mathrm{T}}) = R \tag{8}$$

where R is the measurement noise covariance.

Thus, the parameters can be estimated by the following formulas

$$\hat{\mathbf{x}}_{k+1} = \hat{\mathbf{x}}_k + \mathbf{K}_k(z_k - \mathbf{H}_k \hat{\mathbf{x}}_k) \tag{9}$$

$$\mathbf{K}_k = \mathbf{P}_{k\text{-}1}\mathbf{H}_k^{\mathrm{T}}(\mathbf{H}_k \mathbf{P}_{k\text{-}1}\mathbf{H}_k^{\mathrm{T}} + R)^{-1} \tag{10}$$

$$\mathbf{P}_k = (\mathbf{I} - \mathbf{K}_k \mathbf{H}_k)\mathbf{P}_{k\text{-}1} \tag{11}$$

where $\hat{\mathbf{x}}$ represents the estimate of $\mathbf{x}$, $\mathbf{K}$ and $\mathbf{P}$ denote the Kalman gain and estimate error covariance, respectively, and $\mathbf{I}$ is a unit matrix with respect to the number of parameters. The dimensions of $\mathbf{K}$, $\mathbf{P}$, and $\mathbf{I}$ matrices are in accordance with state vector $\mathbf{x}$.

3.3 Feedback controller

A feedback controller is employed in the proposed method to enhance the robustness and improve the tracking performance of the feedforward controller. To make the proposed method easy to use, the proportional-integral controller (PI controller) is adopted in this study, where it can be expressed as follow

$$d_{\mathrm{c},k}^{\mathrm{FB}} = K_{\mathrm{P}} e_k + K_{\mathrm{I}} \sum e_k \tag{12}$$

where $d_{\mathrm{c},k}^{\mathrm{FB}}$ is the displacement generated by the PI controller, e is the error displacement between d and d_{m}; K_{P} and K_{I} are the proportional and integral gains in PI controller, respectively.

4. Reference structure and controller design

4.1 Overview of the RTHS benchmark problem

Silva *et al*. (2020) established a benchmark problem in RTHS to provide a unified and clear standard for evaluating the performance of various control strategies. In the benchmark problem, a 3-story, 2-bay steel frame is selected as the reference structure, as shown in Fig. 3(a). The part in the red block is taken as NS, while the rest in the blue block is considered PS with a single degree of freedom. The EOM of NS for the benchmark problem is consistent with Eq. (1), in which $\mathbf{f}_{\mathrm{P}} = [-f_{\mathrm{m}}, 0, 0]^{\mathrm{T}}$ and f_{m} denotes measured force from PS. f_{m} is described as follows

$$f_{\mathrm{m}} = m_{\mathrm{P}}\ddot{d}_{\mathrm{m}} + c_{\mathrm{P}}\dot{d}_{\mathrm{m}} + k_{\mathrm{P}} d_{\mathrm{m}} \tag{13}$$

where, m_{P}, c_{P}, and k_{P} are the mass, damping, and stiffness of the PS, respectively.

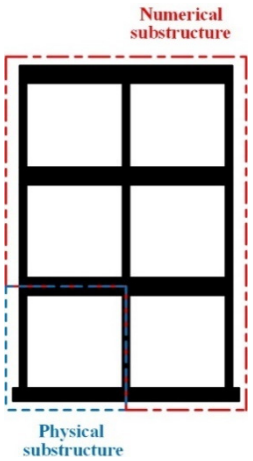

(a) Reference structure and partitioning of substructures

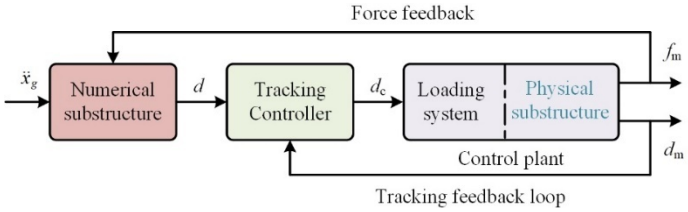

(b) Scheme of RTHS with control in the benchmark problem

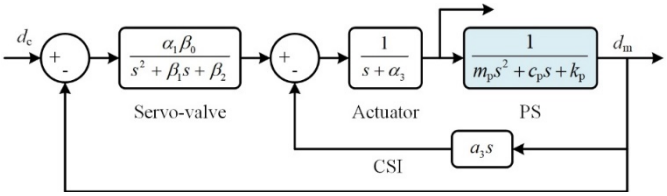

(c) Block diagram of the control plant

Fig. 3 Block diagram of the benchmark problem

Table 1 Parametric values of the control plant (Silva *et al*. 2020)

Component	Parameter	Nominal value	Standard deviation	Units
Actuator	α_2	4.23×10^6	-	m Pa
	α_3	3.3	1.3	1/s
Servo-valve	$\alpha_1\beta_0$	2.13×10^{13}	-	$m\cdot Pa\cdot s^{-1}$
	β_1	425	3.3	nondimensional
	β_2	10×10^4	3.31×10^3	1/s
P	m_P	29.1	-	kg
S	k_P	1.19×10^6	5×10^4	N/m
	c_P	114.6	-	kg/s

Table 2 RTHS partitioning case (Silva *et al*. 2020)

Partitioning configuration	Reference floor mass (kg)	Reference modal damping (%)	Sensitivity of experiment setup to desynchronization
Case 1	1000	5	Slightly sensitive
Case 2	1100	4	Slightly sensitive
Case 3	1300	3	Slightly sensitive
Case 4	1000	3	Slightly sensitive
Case 5	**900**	**2**	**Moderately sensitive**

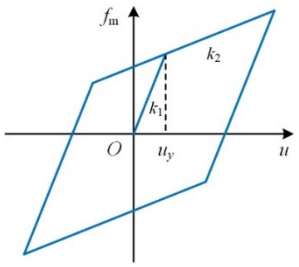

Fig. 4 Bilinear model

Table 3 Parameter values of nonlinear physical substructure models

Nonlinear PS model	Parameters	Value	Units
Bilinear	k_1	1.1688×10^6	N/m
	k_2	5.2596×10^5	N/m
	uy	0.0025	m
Bouc-wen	α_P	0.02	-
	β_P	300	-
	k_e	1.19×10^6	N/m
	γ_P	300	-
	n	1.05	-

Fig. 3(b) shows the flowchart of the benchmark problem. The earthquake acceleration, $\ddot{x}_g$, and the force feedback, f_m, are the input of NS, while the desired displacement, d, is the output of NS, which is calculated using Eq. (1). Then the tracking controller produces the commanded displacement, d_c, by the displacements d, d_c, and d_m. Subsequently, the PS is driven by the loading system using the commanded displacement. Finally, the restoring force, f_m, and d_m from the PS are fed back to the NS and the tracking controller, respectively. The previous steps are repeated till the end of the simulation.

Fig. 3(c) details the model of the control plant, in which the servo-valve, the actuator, and the PS are represented by transfer functions. The parametric values of the control plant are listed in Table 1. Considering the uncertainties in the actuator, servo-valve, and PS, some of the parameters, namely α_3, β_1, β_1, and k_P, are treated as random variables, and they will change each time the program is run. In the following content, the control plant consisting of 'Nominal value' of each parameter is called the nominal model, while that consisting of 'Standard deviation' and 'Nominal value' is regard as the perturbed model. They are used for the robustness investigation of the proposed method.

Table 2 presents the partitioning cases used in this study. Four partitioning cases (Cases 1-4) are provided in the original benchmark problem to investigate the capability of different tacking controllers. An additional case (Case 5) is considered in this study to further investigate the feasibility and robustness of the proposed control method under moderately sensitive conditions. Further, nine evaluation criteria, J_1-J_9, in the benchmark problem are also adopted to quantify the MAC-KF's performance, where the different computational formulas and definitions are shown in Appendix 1.

Moreover, this study considers two types of nonlinear PSs to further evaluate the performance of the proposed control method for nonlinear PS. The force–displacement relationship of the first nonlinear PS is represented by a bilinear model, whose diagram is shown in Fig. 4. In the figure, k_1 and k_2 are the initial and degraded stiffness, respectively, and u_y is the yielding displacement. For another PS, the force–displacement relationship is represented by the Bouc-wen model, described by

$$f_m = \alpha_P k_e u + (1-\alpha_P) k_e E_v \tag{14}$$

$$\dot{E}_v = \dot{u} - \beta_P |\dot{u}| |E_v|^{n-1} E_v - \gamma_P \dot{u} |E_v|^n \tag{15}$$

where E_v denotes the evolutionary variable; α_P, β_P, γ_P, n, and k_e are parameters that define the shape of the hysteretic loop in the Bouc-wen model, u and $\dot{u}$ denote the displacement and velocity of the PS, respectively. Table 3 shows the parameter values of the two nonlinear physical models.

4.2 Controller design

Given that the second-order transfer function can capture sufficient dynamics of the control plant, it was employed to design the feedforward controller. By using the forward difference method, a three-parameter discrete-time feedforward controller is derived, which can be described as

$$d_{c,k}^{FF} = x_{1,k}d_k + x_{2,k}d_{k-1} + x_{3,k}d_{k-2} \quad (16)$$

A preliminary simulation with an uncontrolled control plant was conducted using a sweep signal, with an amplitude and frequency range of 5 mm and 0.1-20 Hz, respectively. The commanded and measured displacements are used to calculate the initial state vector $\mathbf{x}_0$ by the least squares method, resulting in $\mathbf{x}_0 = [5.9645; -8.1154; 3.0736]$. The initial estimate error covariance is given by $\mathbf{P}_0 = \text{diag}([5.9645^2\ 8.1154^2\ 3.0736^2])$ and the measurement noise covariance, R, is set to 10^{-4}. The proportional gain, K_P, and integral gain, K_I, for the feedback controller are set to 8 and 4.5, respectively.

It should be noted, to suppress the negative effect of the measurement noise, a Kalman filter has been employed in this study, because it cannot induce additional time delay to control plant (Ning *et al*. 2020, Shi *et al*. 2016). The design details are omitted due to the length limitation.

4.3 Tracking performance with prescribed displacement

To investigate the tracking performance of the designed controller, open-loop responses are presented in this subsection. Fig. 5 shows that three different specified displacements are considered in this subsection to analyze the tracking performance of the control strategies in the preceding subsection. The displacements are the responses obtained from the benchmark structure under El Centro, Kobe, and Morgan Hill earthquake excitations. Each specified displacement has a duration of 30 s.

Fig. 6 presents the values of J_1-J_3 with the proposed method under the prescribed displacement shown in Fig. 5. To demonstrate the necessity of adaptive control for the benchmark problem, the results of a non-adaptive control strategy, where the adaptive law removed from MAC-KF, are also presented in Fig. 6. It is seen in the figures, the time delay with MAC-KF keeps zero for the three cases, and the J_2 and J_3 values are less than 1.5%, demonstrating the effectiveness of MAC-KF. While for the non-adaptive cases, the time delay is 1 ms, and the J_2 and J_3 values are larger than 2.0%. Compared with non-adaptive cases, the J_1-J_3 of MAC-KF are reduced more than 50%, indicating the time delay is varying, and it is necessary to apply the adaptive strategy to the benchmark problem.

The evolutions of the estimated parameters under the three specified displacement inputs are considered, which are shown in Fig. 7. The figure shows that the estimated parameters adjust rapidly for the first and third simulations in the first 10 s, and these three parameters almost converged to a constant value within 30 s. The estimated parameters reach a relatively stable condition though the convergence trends of parameters are not particularly obvious for displacement inputs 2 and 3.

To quantify the contribution of the feedforward and feedback controls to the overall control signal effort, the time histories of d_c, d_c^{FF}, and d_c^{FB} corresponding to displacement 1 are presented in Fig. 8. It is seen in Fig. 8, the feedforward control signal has a comparable magnitude to the overall signal, while the contribution of the feedback control signal is relatively small, indicating that the feedforward control signal dominates the commanded displacement. Hence, it is necessary to investigate the effect of the settings in the feedforward controller.

5. Parametric analysis

5.1 Effect of initial settings for KF

Section 3 shows that the initial parameters, i.e., the initial state vector, $\mathbf{x}_0$, the initial estimate error covariance,

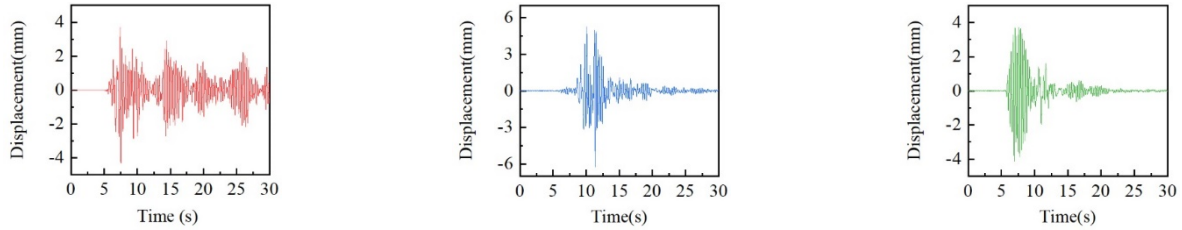

(a) Displacement 1 (b) Displacement 2 (c) Displacement 3

Fig. 5 Prescribed displacement time histories

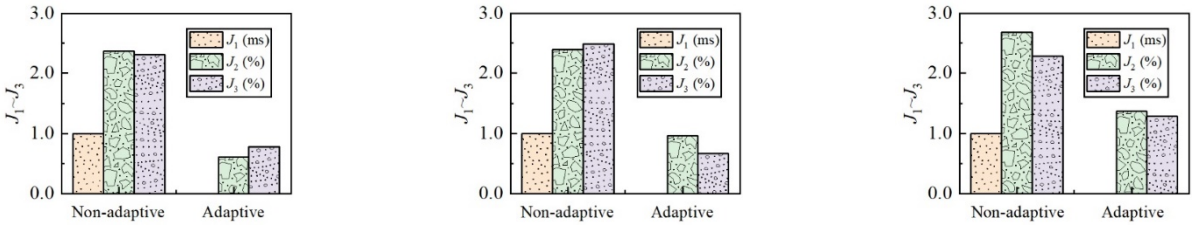

(a) Displacement 1 (b) Displacement 2 (c) Displacement 3

Fig. 6 J_1-J_3 values under prescribed displacements

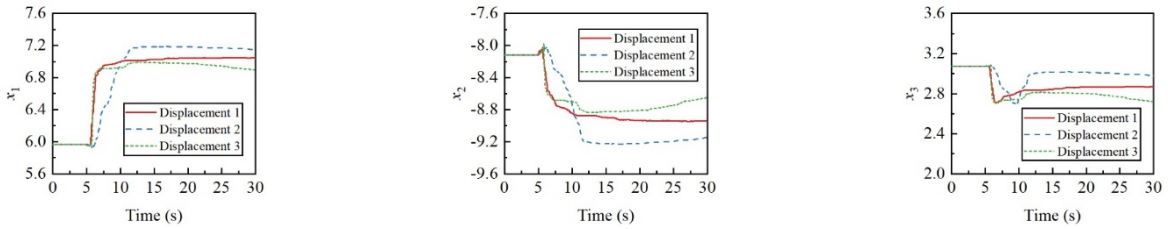

(a) x_1 (b) x_2 (c) x_3

Fig. 7 Evolutions of the estimated CPPs under three specified displacements

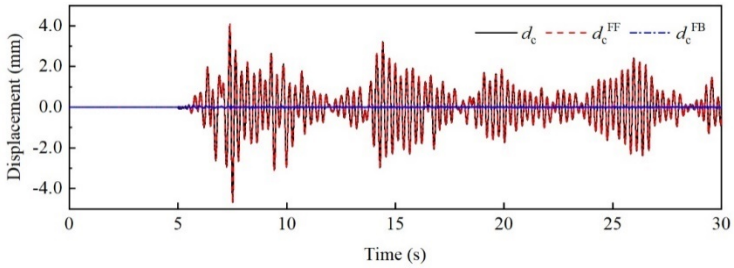

Fig. 8 Time histories of feedforward, feedback, and overall control signals

$\mathbf{P}_0$, and the measurement noise covariance, R, play a significant role in the proposed control method. Thus, numerical simulations were conducted to investigate the effect of the KF on the proposed control strategy. In this study, a parametric expression of the initial parameters is defined as follow

$$W = Q_f W_0 \tag{17}$$

where Q_f is a scaling factor, varying from 0.7 to 1.3 with an increment of 0.05; W_0 represents the values of the initial parameters of KF, as given in subsection 4.2. The parameters that were not investigated for each parametric study were set to their default values. Due to the calculated time delay, J_1, was kept at 0 ms in the simulations, only the evaluation criteria, J_2 to J_3, which are the root mean square of the error and the peak tracking error, were used to quantify the performance of the control strategy. In addition, the feedback controller's gain settings are similar to those in subsection 4.2.

5.1.1 Influence of the initial state vector $\mathbf{x}_0$

Fig. 9 shows the values of J_2 and J_3 between the commanded and measured displacements. The figure shows that although the values of J_2 and J_3 grow as the factor, Q_f, increases, their maximum values are less than 1.5%. Compared with displacement inputs 1 and 2, the changes in the evaluation indexes for the third specified displacement are more obvious. Additionally, the effects of the initial state vector, $\mathbf{x}_0$, on the convergence values of the CPPs were also investigated and are presented in Fig. 10. This figure shows that the converged parameter values increased gradually as the factor, Q_f, increased. The reason can be explained as follows. The feedforward controller is designed using a second-order transfer function model, which is an approximate representation of the control plant. The commanded displacement generated by MAC-KF changed with different initial values, resulting in the dynamics of the control plant in different frequency ranges being excited. It is well-known that the identified simplified numerical models may be varied with different external excitations for complex control plant, leading to the convergence parameter gradually decrease in value as the factor increases.

(a) J_2 (b) J_3

Fig. 9 J_2 and J_3 for different $\mathbf{x}_0$

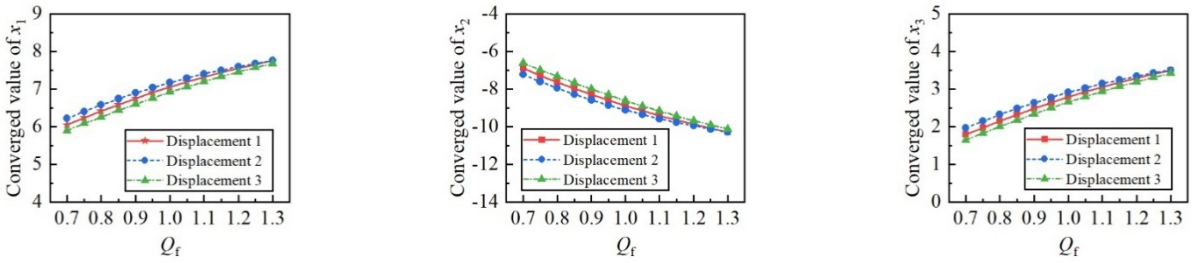

(a) Converged value of x_1 (b) Converged value of x_2 (c) Converged value of x_3

Fig. 10 Effects of $\mathbf{x}_0$ on the converged values of CPPs

(a) J_2 (b) J_3

Fig. 11 J_2 and J_3 for different $\mathbf{P}_0$

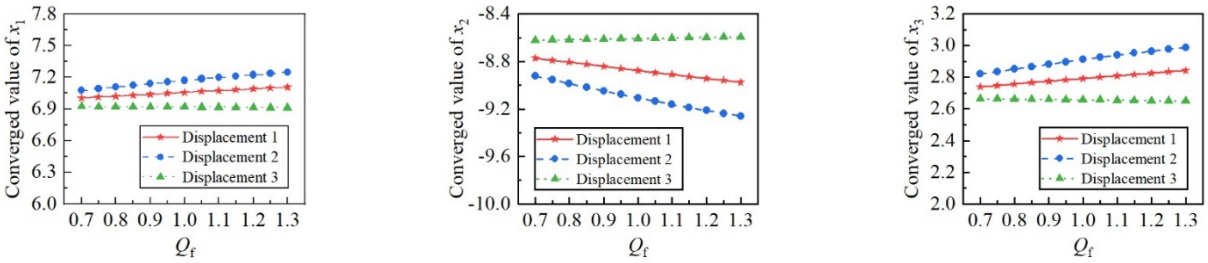

(a) Converged value of x_1 (b) Converged value of x_2 (c) Converged value of x_3

Fig. 12 Effects of $\mathbf{P}_0$ on the converged values of CPPs

5.1.2 Influence of the initial estimate error covariance $\mathbf{P}_0$

Fig. 11 shows the values of J_2 and J_3 with different initial estimate error covariance, $\mathbf{P}_0$. The values of the two indexes under different displacement inputs were almost constant, though Q_f was varied from 0.7 to 1.3. Fig. 12 shows the converged values of the CPPs. The figure shows that the converged values of the estimated parameters under the first displacement input were almost constant. The converged values of parameters for the other two situations increased gradually as Q_f increased. However, the variation ranges of the converged values are all within 10% of the nominal cases (namely $Q_f = 1$). From Figs. 11-12, it can be concluded that the initial estimate error covariance, $\mathbf{P}_0$, has little effect on the performance of the proposed control strategy.

5.1.3 Influence of the measurement noise covariance R

Fig. 13 shows that the values of the J_2 and J_3 for the three displacement inputs were almost the same even though varied, which is similar to those presented in Fig. 11. Fig. 14 shows the converged values of the CPPs with different measurement noise covariance matrix, R. The absolute values of the converged parameters were almost constant under displacement input 3. Although the converged values of the three parameters changed slightly in the first two displacement inputs, the varied range of the converged values is less than 10% of the nominal case of R. The results demonstrate that the tracking performance of the proposed controller is almost independent of the measurement noise covariance, R.

5.2 Effect of the feedback controller

To investigate the effect of the PI controller, K_P is set to range from 2 to 10 with increments of 2, whereas K_I varies from 1 to 5 with increments of 0.5. Thus, 45 simulations (5 × 9) were conducted. Similar to the results in subsection 5.1, J_1 maintain at 0 ms for all simulations, and only J_2 and J_3 are provided to evaluate the performance of the proposed strategy. The parameter settings in KF are identical to those

(a) J_2 (b) J_3

Fig. 13 J_2 and J_3 for different R

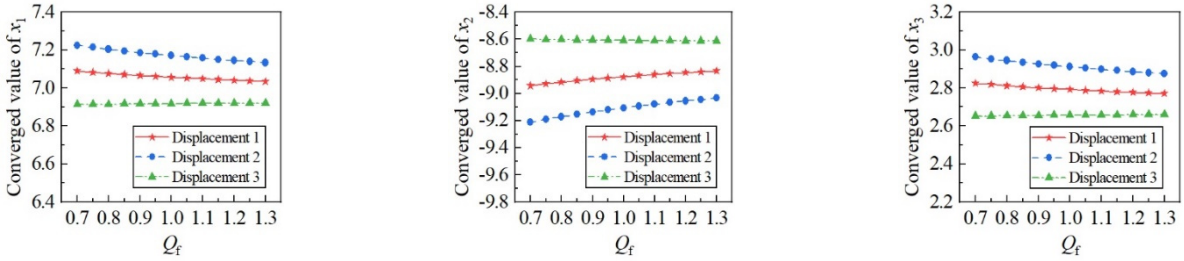

(a) Converged value of x_1 (b) Converged value of x_2 (c) Converged value of x_3

Fig. 14 Effects of R on the converged values of CPPs

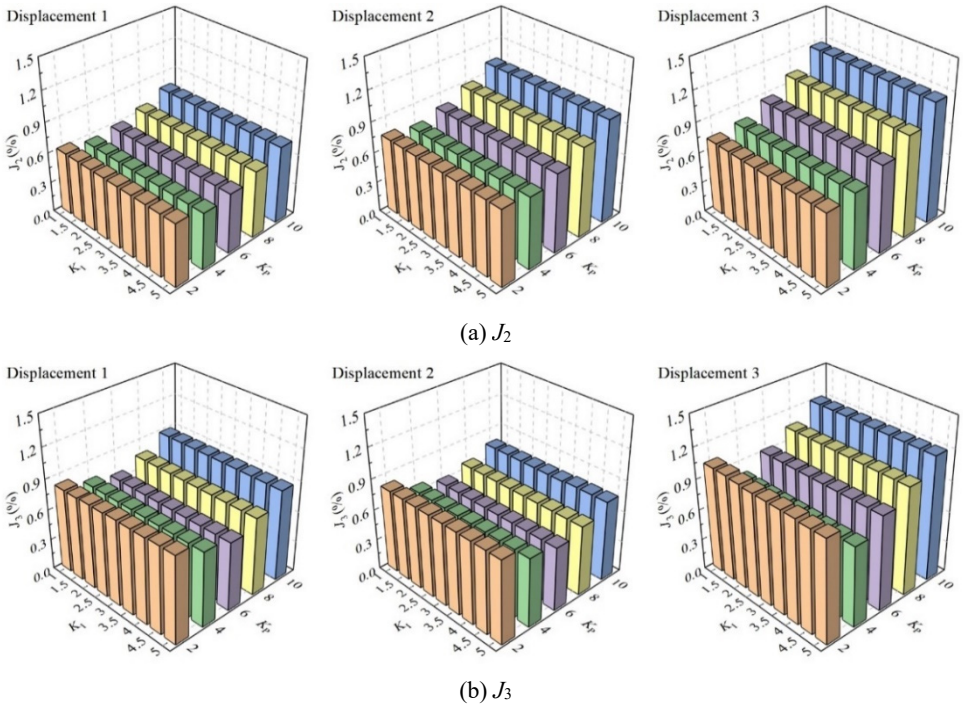

(a) J_2

(b) J_3

Fig. 15 J_2 and J_3 for the different combinations of K_P and K_I

in subsection 4.2.

Fig. 15 lists the values of J_2 and J_3 calculated with different combinations of K_P and K_I under the three prescribed displacements. The figure shows that as K_P increased, the values of J_2 and J_3 decreased first and then increased, and they attained maximum values when $K_P = 4$. However, the values of J_2 and J_3 are almost constant with K_I varying from 1 to 5 for different K_P. This indicates that the effect of K_I can be neglected and K_P affects the tracking performance of the proposed adaptive strategy. A moderate K_P setting can visibly advance the system's response and improve the tracking performance.

Fig. 16 shows the converged values of the CPPs for different combinations of K_P and K_I. The figure shows that as K_P changes, the converged values of CPPs vary in different degrees under three seismic excitations. The

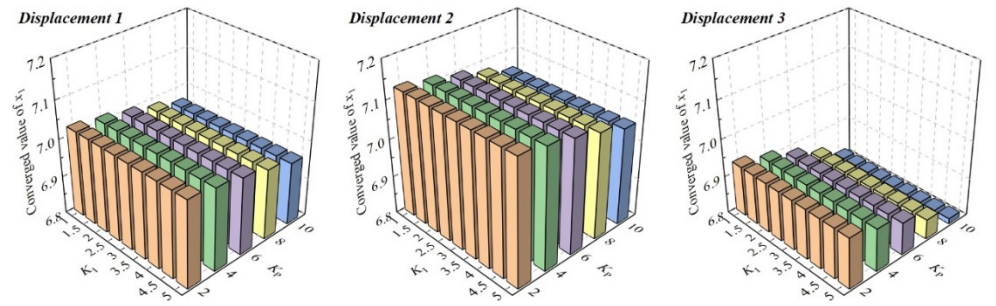

(a) Converged value of x_1

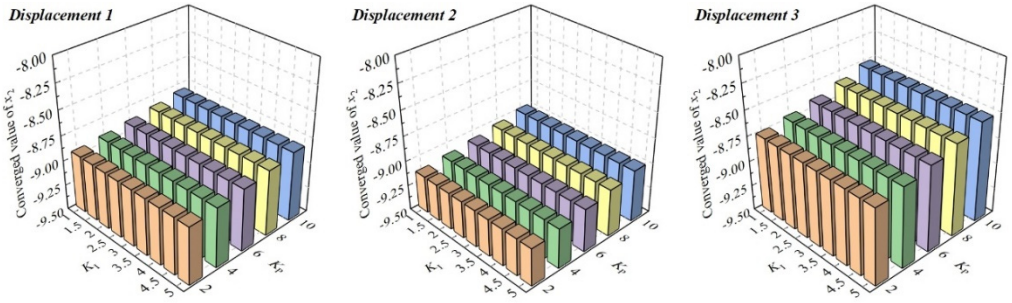

(b) Converged value of x_2

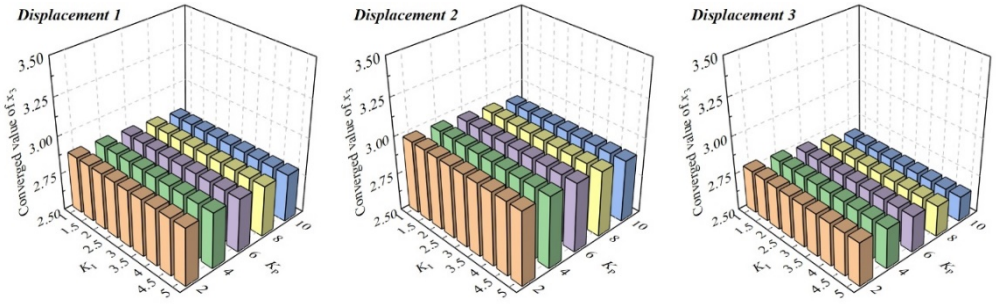

(c) Converged value of x3

Fig. 16 Converged values of the CPPs for the different combinations of K_P and K_I

converged values of parameters x_1 and x_3 gradually decrease, whereas those of x_2 gradually increase. However, as K_I varies, the converged values remain almost constant for a given K_P. This demonstrates that the proportional gain, K_P, has a more obvious effect on the converged values than K_I.

6. Virtual RTHS

6.1 Case I: linear PS

As presented in the previous section, the KF's initial settings had an insignificant effect on the tracking performance of the proposed control strategy, indicating the strong robustness of KF. Virtual RTHS (vRTHS) was conducted using the benchmark problem to further investigate the capability of the proposed method. Three earthquake scenery, such as El Centro, Kobe, and Morgan, are considered and the five partitioning cases shown in Table 2 are included for each earthquake acceleration record.

In addition to the nominal cases, 20 sets of parameters used to account for the model uncertainties of the control plant are randomly generated for each partitioning instance according to the distribution indicated in Table 1. Thus, 315 (3 × 5 × 21) vRTHSs were accomplished in this subsection.

6.1.1 Displacement

Fig. 17 shows the displacement time histories for Case 1 under El Centro earthquake excitation, where the reference and commanded displacements are also provided. As revealed by Fig. 17(a), the displacement measurement is nearly identical to the other two displacements. The displacement errors between the measured and desired displacements are presented in Fig. 17(b) in the form of absolute values, referred to as error 1. By analogy, error 2, the absolute values of the displacement errors between the measured and reference displacements, are presented in Fig. 17(c). Figs. 17(b)-(c) show that the displacement errors are maintained at a relatively low level, suggesting the excellent tracking capability of the MAC-KF control method. Errors 1 and 2 have the largest values at

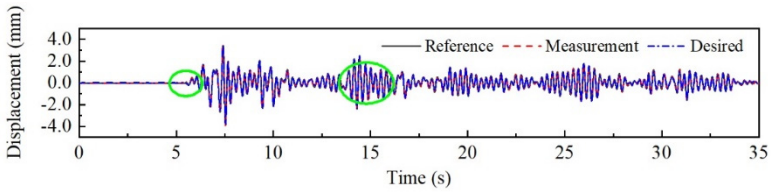

(a) Global view

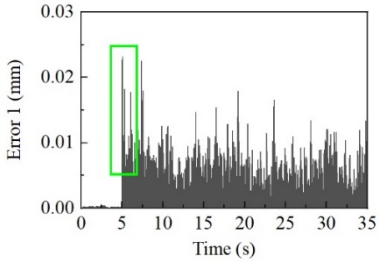

(a) Error 1

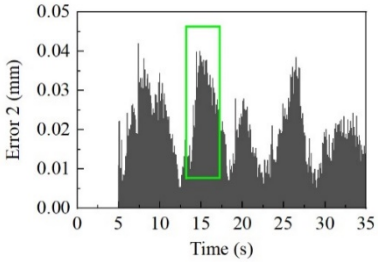

(c) Error 2

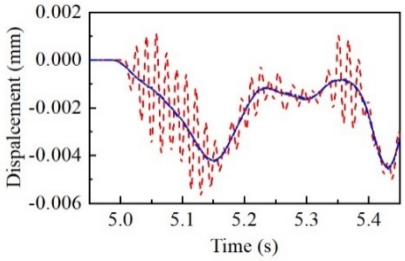

(d) Enlarged view 1

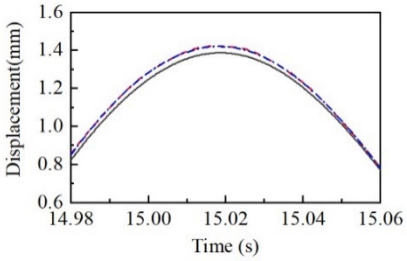

(e) Enlarged view 2

Fig. 17 Displacement time histories under El Centro earthquake excitation (Case 1)

approximately 5 and 15 s, respectively, where the reasons can be illustrated by Figs. 17(d)-(e). As shown in Fig. 17(d), small amplitude fluctuations are observed in the measured displacement, which may cause error 1 having the largest values at around 5 s. It can be seen from Fig. 17(e) that the maximum value of error 2 can be attributed to the amplitude discrepancy and phase error between the reference displacement and the measured one around 15 s.

Table 4 lists the results of nine evaluation criteria using the proposed control approach under the three earthquake excitations. Only Cases 1 and 5 are shown in the table because Cases 2 to 4 are similar to Case 1 for each earthquake acceleration record, and they are represented in Appendix 2. In the table, "Nominal" represents the case where the nominal control plant is employed, while "Mean" and "STD" respectively denote the mean and standard deviation of the 9 evaluation criteria in the 20 perturbed virtual RTHSs for robustness evaluation.

Table 4 shows that the maximum nominal values of J_1 in the three seismic scenarios are not more than 0.13%, and the nominal values of J_2 and J_3 are both less than 2%, indicating the excellent tracking performance of MAC-KF method. For Cases 1 and 5, the mean values of J_1-J_3 are consistent with the nominal values, and their standard values are all less than 1%. This shows that the proposed method can still have an excellent tracking performance and stability for the control plant under disturbed conditions. The table also shows that the values of J_1-J_3 generated by Case 5 are much lower than those of Case 1, indicating that the method can still accurately identify the error between the desired displacement and the measured displacement, decreasing the time delay of the control plant under moderately sensitive conditions.

In the benchmark problem, the evaluation criteria J_4-J_9 are used to evaluate the global performance of the proposed strategy. For J_4-J_9, the 'Nominal' values of Case 1 and 5 are almost identical to the 'Mean' values of these two cases under each seismic excitation, and the 'STD' values of Case 1 and 5 are lower than 2%. In general, the evaluation criteria of Case 5 are higher than those of Case 1 for each earthquake excitation, but the maximum 'Nominal' and 'Mean' values of Case 5 are less than 6%. Thus, the proposed control strategy has relatively stable global performance in slightly and moderately sensitive conditions.

6.1.2 Parameter estimation

The evolutions of the estimated parameters for Case 1 under El Centro earthquake record are shown in Fig. 18. The figure shows that the estimated parameters remained unchanged in the first 5 s because there is no earthquake input, thus the displacement command and measurement are almost zero. As the earthquake increased, the discrepancies between the commanded and measured displacements appeared immediately, and the estimated parameters responded rapidly by the KF algorithm to adjust the commanded displacement sent to the control plant. The

Table 4 vRTHS evaluation criteria for the proposed control method

Control/compensation Method	Case	Statistical algorithm	J_1 (ms)	J_2 (%)	J_3 (%)	J_4 (%)	J_5 (%)	J_6 (%)	J_7 (%)	J_8 (%)	J_9 (%)
El Centro	Case 1	Nominal	0.00	0.91	0.98	2.03	1.24	1.78	1.78	0.90	0.89
		Mean	0.08	1.11	**1.33**	2.39	1.86	1.97	1.98	1.24	1.25
		STD	0.13	0.24	0.43	0.69	0.69	0.81	0.81	0.61	0.62
	Case 5	Nominal	0.00	0.56	0.84	5.61	3.17	5.54	5.55	3.02	3.01
		Mean	0.03	0.64	0.95	5.92	3.56	5.85	5.85	3.39	3.38
		STD	0.07	0.13	0.22	1.56	1.24	1.61	1.62	1.30	1.28
Kobe	Case 1	Nominal	0.00	1.31	0.67	1.84	0.90	1.28	1.28	0.80	0.80
		Mean	0.06	1.48	0.77	2.06	1.10	1.44	1.44	0.88	0.87
		STD	0.09	0.14	0.17	0.31	0.22	0.49	0.49	0.26	0.26
	Case 5	Nominal	0.00	1.07	0.81	3.65	2.36	3.48	3.49	2.19	2.18
		Mean	0.02	1.15	0.83	3.71	2.31	3.48	3.49	2.16	2.15
		STD	0.06	0.20	0.20	0.51	0.32	0.62	0.62	0.38	0.38
Morgan Hill	Case 1	Nominal	0.00	**1.66**	1.23	2.49	1.65	1.88	1.89	1.53	1.52
		Mean	0.12	1.83	1.42	3.10	2.32	2.38	2.38	1.98	1.98
		STD	**0.18**	0.35	0.50	1.08	1.03	1.27	1.27	1.01	1.01
	Case 5	Nominal	0.00	0.97	0.79	5.51	4.77	5.40	5.40	4.66	4.66
		Mean	0.04	1.04	0.89	5.91	5.06	5.80	5.80	4.93	4.94
		STD	0.08	0.14	0.12	1.84	1.45	1.95	1.95	1.49	1.49

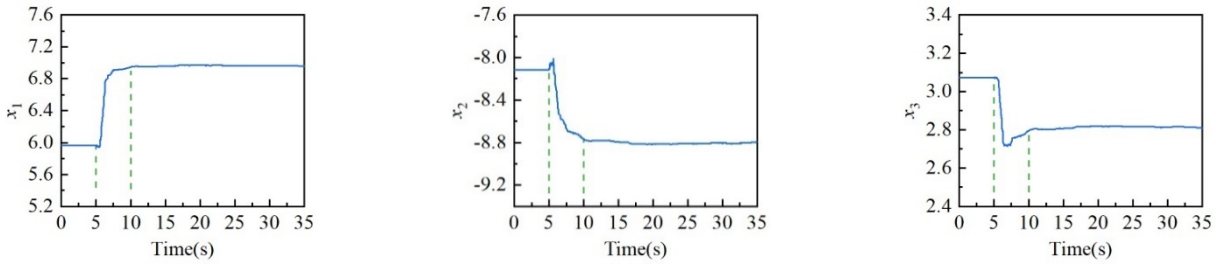

(a) x_1 (b) x_2 (c) x_3

Fig. 18 Evolutions of the estimated CPPs under El Centro earthquake excitation (Case 1)

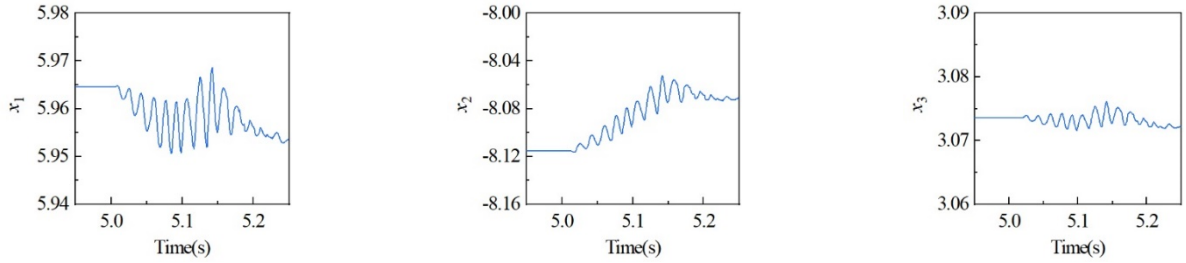

(a) x_1 (b) x_2 (c) x_3

Fig. 19 Enlarged views of the estimated parameters around 5 s

estimated parameters nearly reached a constant value at around 10 s. Notably, the evolutions of the estimated parameters for Morgan and Kobe are not presented because they are similar to those shown in Fig. 18.

The enlarged views of the estimated parameters around 5 s are shown in Fig. 19, where the parameter identifications have a small fluctuation phenomenon for x_1 to x_3. Comparing Figs. 17(b) and 19, it can be found that the estimator cannot completely identify the CPPs due to the lack of sufficient experimental data at the beginning of the simulation. This causes CPPs with errors to be fed back to the feedforward controller, and result in the error between

the desired displacement and the measured one. Then, the proposed controller can continually adjust the values of the desired displacement and the measured one. Then, the proposed controller can continually adjust the values of parameters in real-time to minimize the displacement error.

6.1.3 Comparison with existing method

To demonstrate the superb performance of the proposed control method, four different control or compensation strategies, namely the adaptive feedforward and feedback compensation method (AFF) (Ning *et al*. 2022), KF-based adaptive delay compensation method (KF-ADC) (Ning *et al*. 2020), robust linear-quadratic-gaussian controller (RLQG) (Zhou *et al*. 2019), and tracking error-based adaptive compensator (TE-AC) (Tao and Mercan 2019), are considered in this study. The AFF method adopted the initial parameters of the proposed approach, which is $\mathbf{x}_0$ = [5.9645; −8.1154; 3.0736]; analogously, the initial estimation error covariance is given by $\mathbf{P}_0$ = diag([5.9645^2 8.1154^2 3.0736^2]). The simulation results of the other three methods, KF-ADC, RLQG, and TE-AC, are collected from the published paper by Ning *et al*. (2020), Zhou *et al*. (2019), and Tao and Mercan (2019), respectively.

Table 5 presents the values of J_1-J_9 using five different control/compensation approaches for Cases 1-4 under the El Centro earthquake acceleration record. In the table, "ARN" represents the average of Cases 1-4 where the nominal control plant is used, while "Mean" and "STD" are the mean and standard deviation of the evaluation criteria in all perturbed virtual RTHSs, respectively.

It can be seen from the table, no obvious difference can be detected between the "ARN" and "Mean" of the aforementioned control strategies. Moreover, the "STD" of J_1-J_3 is significantly lower than 1% in all comparative control methods, indicating their outstanding tracking performance. For J_4-J_9, the KF-ADC, RLQG, and MAC-KF are superior to the remaining two methods in general terms. Compared with the AFF and KF-ADC, the MAC-KF has the smallest J_4-J_9. This can be attributed to two main reasons: (i) the higher quasi-certainty and faster response speed of the KF algorithm in parametric estimation; (ii) the robustness improvement caused by the feedback controller. Further, the table shows that the RLQG has the smallest "STD," indicating the superior robustness of this method. However, the "ARN" and "Mean" of the RLQG are larger than those of the MAC-KF. Thus, the MAC-KF has excellent tracking and global performance.

6.2 Case II: nonlinear physical substructure

The previous two subsections present the tracking performance of the proposed controller with a linear physical substructure. However, the variable time delay generated by the nonlinear physical substructure should not be ignored. Several vRTHSs with two nonlinear physical substructures are conducted in the benchmark problem to further investigate the tracking performance and robustness of the proposed method. The control strategy outlined by 4.2 is considered in this subsection. A total of 315 vRTHSs are conducted for the bilinear and Bouc-wen models in this subsection using settings identical to those in subsection 6.1.

Table 6 lists the nine evaluation criteria results in the vRTHS with two nonlinear physical substructures. The descriptions of "ARN," "Mean," and "STD" are the same as those in Table 5. For J_1-J_3, the results of Bilinear or Bouc-wen model show a minor difference in "ARN" compared with that in "Mean," and all "STD" are not more than 1%. Although the "STD" of the bilinear model for J_4-J_9 is mostly above 1%, there is no significant discrepancy in the bilinear model's "ARN" and "Mean." The Bouc-wen model's J_4-J_9 results exceed those in the bilinear model,

Table 5 Comparative evaluation criteria for Cases 1-4 under El Centro earthquake excitation

Control/compensation Method	Statistical algorithm	J_1 (ms)	J_2 (%)	J_3 (%)	J_4 (%)	J_5 (%)	J_6 (%)	J_7 (%)	J_8 (%)	J_9 (%)
TE-AC	ARN	1.30	4.87	5.48	19.05	10.95	14.06	17.24	9.24	9.34
	Mean	1.33	4.91	5.51	19.34	11.10	14.33	17.51	9.36	9.47
	STD	0.23	0.58	0.46	6.10	2.44	1.89	5.88	2.81	2.76
AFF	ARN	1.00	2.17	2.21	9.17	5.28	8.86	8.88	5.05	5.06
	Mean	0.97	2.22	2.32	9.31	5.50	8.98	9.00	5.22	5.23
	STD	0.28	0.47	0.74	3.00	2.06	3.02	3.02	2.12	2.13
KF-ADC	ARN	0.20	0.97	1.37	4.37	2.84	4.08	4.09	2.42	2.42
	Mean	0.30	1.22	1.82	5.03	3.48	4.66	4.67	2.89	2.90
	STD	0.27	0.37	0.48	2.83	1.48	2.93	2.93	1.52	1.50
RLQG	ARN	0.00	2.40	2.08	3.32	2.65	2.21	2.21	1.27	1.27
	Mean	0.00	2.40	2.08	3.34	2.66	2.23	2.23	1.28	1.28
	STD	0.00	0.45	0.29	0.27	0.12	0.56	0.56	0.36	0.36
MAC-KF	ARN	0.00	0.80	0.91	2.48	1.50	2.30	2.30	1.28	1.29
	Mean	0.06	0.95	1.17	2.67	1.87	2.40	2.41	1.46	1.47
	STD	0.11	0.23	0.32	0.84	0.61	0.97	0.97	0.65	0.65

Table 6 evaluation criteria in vRTHS with two nonlinear physical substructures

Physical substructure	Statistical algorithm	J_1 (ms)	J_2 (%)	J_3 (%)	J_4 (%)	J_5 (%)	J_6 (%)	J_7 (%)	J_8 (%)	J_9 (%)
Bilinear	ARN	0.00	2.27	5.31	3.93	5.28	3.30	3.29	1.95	1.93
	Mean	0.05	2.37	5.30	4.16	5.29	3.48	3.47	2.12	2.10
	STD	0.12	0.64	0.81	1.25	0.61	1.50	1.51	0.87	0.88
Bouc-wen	ARN	0.00	2.98	5.58	4.76	6.57	3.75	3.68	3.73	3.60
	Mean	0.02	3.15	5.67	7.69	7.81	7.04	7.01	5.60	5.51
	STD	0.07	0.79	1.00	3.85	4.38	4.13	4.10	3.94	3.77

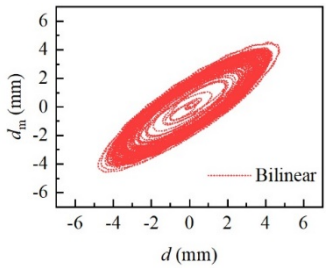

(a) d_m versus d without control of Bilinear

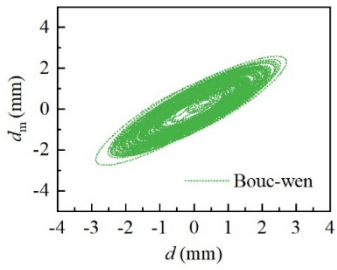

(b) d_m versus d without control in Bouc-wen

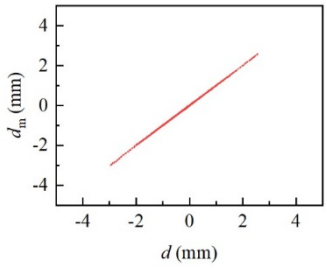

(c) d_m versus d with control in Bilinear

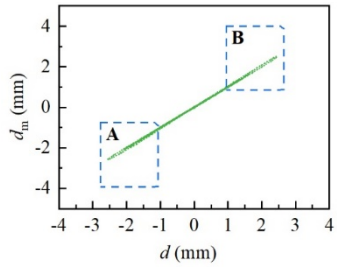

(d) d_m versus d with control in Bouc-wen

Fig. 20 Displacement contrast without/with control under El Centro seismic excitation

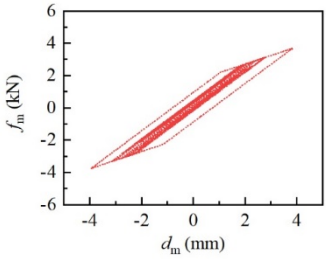

(a) Bilinear

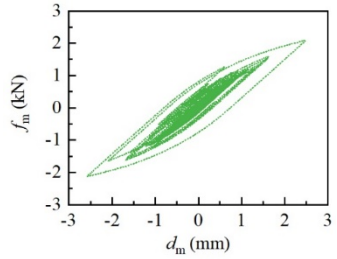

(b) Bouc-wen

Fig. 21 Hysteresis loops with nonlinear physical substructures under El Centro seismic excitation

which can be attributed to the PS's significantly larger nonlinearity with the Bouc-wen model. The aforementioned discussions can be used to draw the following conclusions: (i) the MAC-KF control method has excellent tracking performance for the PS with either the bilinear model or the Bouc-wen model; (ii) the global performance of the MAC-KF control method under the bilinear model is greater than that under the Bouc-wen model; (iii) the "STD" results indicate that the proposed control strategy exhibits superb robustness in the tracking performance, particularly for the Bilinear model.

Fig. 20 shows the relationships of the desired displacement, d, versus the measurement displacement, d_m, with/without control strategy for the two nonlinear PSs under El Centro earthquake acceleration record. The figure shows obvious de-synchronization between d and d_m for the cases without an additional controller. However, the relationships between d and d_m, with the proposed controller, are almost linear with one slope, demonstrating the outstanding tracking ability of the proposed strategy for

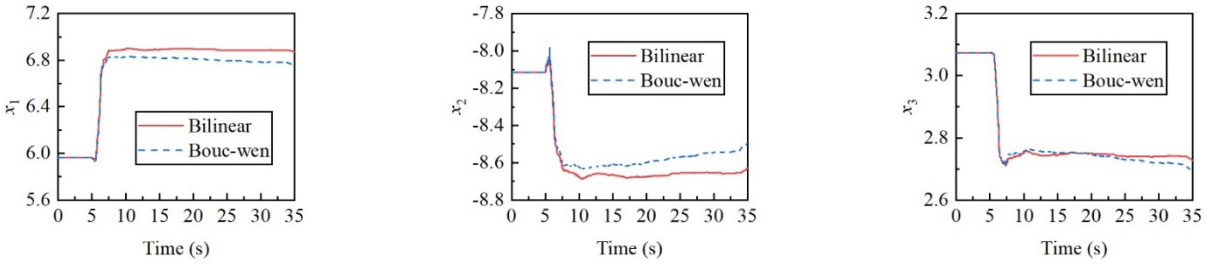

(a) x_1 (b) x_2 (c) x_3

Fig. 22 Evolutions of the estimated CPPs with nonlinear PS

dealing with the nonlinear control plant. However, the A and B portions of Fig. 20(d) depict a slight de-synchronization between d and d_m. This is mainly caused by the stronger nonlinearity of the physical substructure with the Bouc-wen model, which can be .further verified by the hysteresis loops in Fig. 21.

Fig. 21 present the hysteresis loops between the feedback force, f_m, and the measurement displacement, d_m, for the two nonlinear physical substructures under the El Centro earthquake acceleration record, respectively. The figure shows that the physical substructures suffered a significant nonlinearity in vRTHSs and that this nonlinearity of the physical substructure is even more pronounced when the Bouc-wen model is used. Further, there is extremely high synchronization between d and d_m with the control strategy (Fig. 20) and small values of the nine evaluation criteria (Table 6), demonstrating that the proposed strategy has excellent tracking performance and robustness.

Fig. 22 presents the evolutions of the estimated parameters with nonlinear PS. The evolution trends are almost similar to those in the linear PS cases, namely the estimated parameters remained unchanged in the first 5 s and followed by a rapidly adjustment, and then reached almost constant values. While for parameters x_2 and x_3 after 10 s, there are obvious fluctuates. That is to say, the control plant model is time-varying, because the PS suffered nonlinearities in different degrees. The reason for the parameters seem unchanged after 10 s is that, the primary time delay has been remedied by the estimated CPPs and the residual time delay is very small, thus the estimated parameters varied in a small range.

This study proposes a model-based adaptive control strategy using KF to address the variable time delay, mainly caused by the dynamics of the servo-hydraulic actuator and physical specimen, and the data transmission. Simulations with prescribed displacement and vRTHSs were carried out to investigate the capability and robustness of the proposed method. The main conclusions are as follows:

- The principle of the proposed adaptive control method, referred to as MAC-KF, was provided. The parameterized feedforward controller is designed by the discrete inverse model of the control plant, whose parameters are estimated and updated by the KF filter. A feedback controller is adopted to improve the control method's robustness.
- The tracking performance and parametric study of the proposed method were investigated using three specified displacements. The absolute values of the displacement errors are less than 0.05 mm, and the estimated CPPs can adjust rapidly and converge eventually. The parametric study demonstrated that the initial state vector $\mathbf{x}_0$ had a more pronounced effect on the tracking performance and converged values of the CPPs than the initial estimate error covariance, $\mathbf{P}_0$, and the measurement noise covariance, R.
- The feasibility of the proposed control method is verified by vRTHSs via the benchmark problem, using linear and nonlinear PSs. The results of the vRTHS demonstrated that the proposed adaptive control approach exhibited excellent tracking performance and robustness. In addition, the contrastive results with the other four control/ compensation strategies revealed that the proposed method not only had strong robustness but also reduced the dependence on the control plant. Moreover, the proposed method still exhibited outstanding tracking ability for the nonlinear control plant.

Acknowledgments

The authors gratefully acknowledge the financial support provided by the National Natural Science Foundation of China [grant numbers 51908231 and 51978213], the Fundamental Research Funds for the Central Universities of Huaqiao University [grant number ZQN-912], Natural Science Foundation of Fujian Province [grant number 2020J01058], and the scientific research fund of Huaqiao University [grant number 18BS306].

References

Blakeborough, A., Williams, M.S., Darby, A.P. and Williams, D.M. (2001), "The development of real–time substructure testing", *Philosophical Transactions of the Royal Society of London. Series A*: *Mathe*. *Phys*. *Eng*. *Sci*., **359**(1786), 1869-1891. https://doi.org/10.1098/rsta.2001.0877

Chen, P.C. and Chen, P.C. (2020), "Robust stability analysis of real-time hybrid simulation considering system uncertainty and delay compensation", *Smart Struct*. *Syst*., *Int*. *J*., **25**(6), 719-

732. https://doi.org/10.12989/sss.2020.25.6.719
Carrion, J. and Spencer Jr., B.F. (2007), *Model-based Strategies for Real-time Hybrid Testing*, University of Illinois at Urbana-Champaign, Urbana-Champaign, IL, USA.
Carrion, J. and Spencer Jr., B.F. (2008), "Real-time hybrid testing using model-based delay compensation", *Smart Struct. Syst., Int. J.*, **4**(6), 809-828. https://doi.org/10.12989/sss.2008.4.6.809
Chae, Y., Kazemibidokhti, K. and Ricles, J.M. (2013), "Adaptive time series compensator for delay compensation of servo-hydraulic actuator systems for real-time hybrid simulation", *Earthq. Eng. Struct. Dyn.*, **42**(11), 1697-1715. https://doi.org/10.1002/eqe.2294
Chen, C. and Ricles, J.M. (2009), "Improving the inverse compensation method for real-time hybrid simulation through a dual compensation scheme", *Earthq. Eng. Struct. Dyn.*, **38**(10), 1237-1255. https://doi.org/10.1002/eqe.904
Chen, C. and Ricles, J.M. (2010), "Tracking error-based servohydraulic actuator adaptive compensation for real-time hybrid simulation", *J. Struct. Eng.*, **136**(4), 432-440. https://doi.org/10.1061/(ASCE)ST.1943-541X.0000124
Chen, C., Ricles, J.M. and Guo, T. (2012), "Improved Adaptive Inverse Compensation Technique for Real-Time Hybrid Simulation", *J. Eng. Mech.*, **138**(12), 1432-1446. https://doi.org/10.1061/(ASCE)EM.1943-7889.0000450
Chen, P., Chang, C., Spencer Jr., B.F. and Tsai, K. (2015), "Adaptive model-based tracking control for real-time hybrid simulation", *Bull. Earthq. Eng.*, **13**(6), 1633-1653. https://doi.org/10.1007/s10518-014-9681-2
Chen, C., Yang, Y., Hou, H., Peng, C. and Xu, W. (2022), "Real-time hybrid simulation with multi-fidelity Co-Kriging for global response prediction under structural uncertainties", *Earthq. Eng. Struct. Dyn.*, **51**(11), 2591-2609. https://doi.org/10.1002/eqe.3690
Darby, A.P., Williams, M.S. and Blakeborough, A. (2002), "Stability and delay compensation for real-time substructure testing", *J. Eng. Mech.*, **128**(12), 1276-1284. https://doi.org/10.1061/(ASCE)0733-9399(2002)128:12(1276)
Drazin, P L. and Govindjee, S. (2017), "Hybrid simulation theory for a classical nonlinear dynamical system", *J. Sound Vib.*, **392**, 240-259. https://doi.org/10.1016/j.jsv.2016.12.034
Gálmez, C. and Fermandois, G. (2022), "Robust adaptive model-based compensator for the real-time hybrid simulation benchmark", *Struct. Control Health Monitor.*, **29**(7). https://doi.org/10.1002/stc.2962
Gao, X.Y., Castaneda, N. and Dyke, S.J. (2013), "Real time hybrid simulation: from dynamic system, motion control to experimental error", *Earthq. Eng. Struct. Dyn.*, **42**(6), 815-832. https://doi.org/10.1002/eqe.2246
Hakuno, M., Shidawara, M. and Hara, T. (1969), "Dynamic destructive test of a cantilever beam, controlled by an analog-computer", *Proceedings of the Japan Society of Civil Engineers*, **1969**(171), 1-9. https://doi.org/10.2208/jscej1969.1969.171_1
Horiuchi, T. and Konno, T. (2001), "A new method for compensating actuator delay in real–time hybrid experiments", *Philosophical Transactions of the Royal Society of London. Series A: Math. Phys. Eng. Sci.*, **359**(1786), 1893-1909. https://doi.org/10.1098/rsta.2001.0878
Horiuchi, T., Inoue, M., Konno, T. and Namita, Y. (1999), "Real-time hybrid experimental system with actuator delay compensation and its application to a piping system with energy absorber", *Earthq. Eng. Struct. Dyn.*, **10**(28), 1121-1141. https://doi.org/10.1002/(SICI)1096-9845(199910)28:10<1121::AID-EQE858>3.0.CO;2-O
Huang, L., Chen, C., Guo, T. and Chen, M.H. (2019), "Stability analysis of real-time hybrid simulation for time-varying actuator delay using the Lyapunov-Krasovskii functional approach", *J. Eng. Mech.*, **145**(1). https://doi.org/10.1061/(ASCE)EM.1943-7889.0001550
Li, H., Maghareh, A., Montoya, H., Uribe, J.W.C., Dyke, S.J. and Xu, Z. (2021), "Sliding mode control design for the benchmark problem in real-time hybrid simulation", *Mech. Syst. Signal Process.*, **151**, 107364. https://doi.org/10.1016/j.ymssp.2020.107364
Li, H., Maghareh, A., Wilfredo Condori Uribe, J., Montoya, H., Dyke, S.J. and Xu, Z. (2022), "An adaptive sliding mode control system and its application to real-time hybrid simulation", *Struct. Control Health Monitor.*, **29**(1), e2851. https://doi.org/10.1002/stc.2851
Marsico, M.R. (2014), "Effects of interface delay in real-time dynamic substructuring tests on a cable for cable-stayed bridge", *Smart Struct. Syst., Int. J.*, **14**(6), 1173-1196. https://doi.org/10.12989/sss.2014.14.6.1173
Nakashima, M. (2020), "Hybrid simulation: An early history", *Earthq. Eng. Struct. Dyn.*, **49**(10), 949-962. https://doi.org/10.1002/eqe.3274
Nakashima, M., Kato, H. and Takaoka, E. (1992), "Development of real-time pseudo dynamic testing", *Earthq. Eng. Struct. Dyn.*, **21**(1), 79-92. https://doi.org/10.1002/eqe.4290210106
Najafi, A. and Spencer Jr., B.F. (2019), "Adaptive model reference control method for real-time hybrid simulation", *Mech. Syst. Signal Process.*, **132**, 183-193. https://doi.org/10.1016/j.ymssp.2019.06.023
Najafi, A. and Spencer Jr., B.F. (2021), "Multiaxial Real-Time Hybrid Simulation for Substructuring with Multiple Boundary Points", *J. Struct. Eng.*, **147**(11), 05021007. https://doi.org/10.1061/(ASCE)ST.1943-541X.0003138
Ning, X., Wang, Z., Zhou, H., Wu, B., Ding, Y. and Xu, B. (2019), "Robust actuator dynamics compensation method for real-time hybrid simulation", *Mech. Syst. Signal Process.*, **131**, 49-70. https://doi.org/10.1016/j.ymssp.2019.05.038
Ning, X., Wang, Z. and Wu, B. (2020), "Kalman filter-based adaptive delay compensation for benchmark problem in real-time hybrid simulation", *Appl. Sci.*, **10**(20), 7101. https://doi.org/10.3390/app10207101
Ning, X., Wang, Z., Wang, C. and Wu, B. (2022), "Adaptive feedforward and feedback compensation method for real-time hybrid simulation based on a discrete physical testing system model", *J. Earthq. Eng.*, **26**(8), 3841-3863. https://doi.org/10.1080/13632469.2020.1823912
Ou, G., Dyke, S.J. and Prakash, A. (2017), "Real time hybrid simulation with online model updating: An analysis of accuracy", *Mech. Syst. Signal Process.*, **84**, 223-240. https://doi.org/10.1016/j.ymssp.2016.06.015
Ouyang, Y., Shi, W., Shan, J. and Spencer Jr., B.F. (2019), "Backstepping adaptive control for real-time hybrid simulation including servo-hydraulic dynamics", *Mech. Syst. Signal Process.*, **130**, 732-754. https://doi.org/10.1016/j.ymssp.2019.05.042
Peiris, L.D.H., du Bois, J.L. and Plummer, A.R. (2021), "Passivity-based adaptive delay compensation for real-time hybrid tests", *Proceedings of the Institution of Mechanical Engineers, Part I: J. Syst. Control Eng.*, **235**(3), 427-432. https://doi.org/10.1177/0959651820945515
Phillips, B.M. and Spencer Jr., B.F. (2013), "Model-based feedforward-feedback actuator control for real-time hybrid simulation", *J. Struct. Eng.*, **139**(7), 1205-1214. https://doi.org/10.1177/0959651820945515
Qian, Y., Ou, G., Maghareh, A. and Dyke, S.J. (2014), "Parametric identification of a servo-hydraulic actuator for real-time hybrid simulation", *Mech. Syst. Signal Process.*, **48**(1-2), 260-273. https://doi.org/10.1016/j.ymssp.2014.03.001
Shao, X. and Reinhorn, A.M. (2012), "Development of a controller platform for force-based real-time hybrid simulation", *J. Earthq. Eng.*, **16**(2), 274-295.

https://doi.org/10.1080/13632469.2011.597487
Shi, P., Wu, B., Spencer Jr., B.F., Phillips, B.M. and Chang, C.M. (2016), "Real-time hybrid testing with equivalent force control method incorporating Kalman filter", *Struct. Control Health Monitor.*, **23**(4), 735-748. https://doi.org/10.1002/stc.1808
Silva, C.E., Gomez, D., Maghareh, A., Dyke, S.J. and Spencer Jr., B.F. (2020), "Benchmark control problem for real-time hybrid simulation", *Mech. Syst. Signal Process.*, **135**, 106381. https://doi.org/10.1016/j.ymssp.2019.106381
Tao, J. and Mercan, O. (2019), "A study on a benchmark control problem for real-time hybrid simulation with a tracking error-based adaptive compensator combined with a supplementary proportional-integral-derivative controller", *Mech. Syst. Signal Process.*, **134**, 106346. https://doi.org/10.1016/j.ymssp.2019.106346
Wallace, M.I., Sieber, J., Neild, S.A., Wagg, D.J. and Krauskopf, B. (2005), "Stability analysis of real-time dynamic substructuring using delay differential equation models", *Earthq. Eng. Struct. Dyn.*, **34**(15), 1817-1832. https://doi.org/10.1002/eqe.513
Wang, Z., Wu, B., Bursi, O.S., Xu, G. and Ding, Y. (2014), "An effective online delay estimation method based on a simplified physical system model for real-time hybrid simulation", *Smart Struct. Syst., Int. J.*, **14**(6), 1247-1267. https://doi.org/10.12989/.2014.14.6.1247
Wang, Z., Ning, X., Xu, G., Zhou, H. and Wu, B. (2019), "High performance compensation using an adaptive strategy for real-time hybrid simulation", *Mech. Syst. Signal Process.*, **133**, 106262. https://doi.org/10.1016/j.ymssp.2019.106262
Wang, Z., Xu, G., Li, Q. and Wu, B. (2020), "An adaptive delay compensation method based on a discrete system model for real-time hybrid simulation", *Smart Struct. Syst., Int. J.*, **25**(5), 569-580. https://doi.org/10.12989/sss.2020.25.5.569
Xu, D., Zhou, H., Shao, X. and Wang, T. (2019), "Performance study of sliding mode controller with improved adaptive polynomial-based forward prediction", *Mech. Syst. Signal Process.*, **133**, 106263. https://doi.org/10.1016/j.ymssp.2019.106263
Zhao, J., French, C., Shield, C. and Posbergh, T. (2003), "Considerations for the development of real-time dynamic testing using servo-hydraulic actuation", *Earthq. Eng. Struct. Dyn.*, **32**(11), 1773-1794. https://doi.org/10.1002/eqe.301
Zhou, Z. and Li, N. (2021), "Improving model-based compensation method for real-time hybrid simulation considering error of identified model", *J. Vib. Control*, **27**(21-22), 2523-2535. https://doi.org/10.1177/1077546320961622
Zhou, H., Xu, D., Shao, X., Ning, X. and Wang, T. (2019), "A robust linear-quadratic-gaussian controller for the real-time hybrid simulation on a benchmark problem", *Mech. Syst. Signal Process.*, **133**, 106260. https://doi.org/10.1016/j.ymssp.2019.106260

Appendix 1 Performance evaluation criteria

Description	Criterion
Tracking time delay	$J_1 = {}_h\left(\sum_k d_k d_{\mathrm{m},k\text{-}h}\right)$
Root mean square of error (*RMSE*)	$J_2 = \sqrt{\frac{\sum_{k=1}^{j}(d_k - d_{\mathrm{m},k})^2}{\sum_{k=1}^{j}(d_k)^2}} \times 100\%$
Peaking tracking error (*PTE*)	$J_3 = \frac{\max\lvert d_k - d_{\mathrm{m},k}\rvert}{\max\lvert d_k\rvert} \times 100\%$
RMSE at the *l*-th floor*	$J_{l+3} = \sqrt{\frac{\sum_{k=1}^{j}[\mathbf{x}_{\mathrm{R},k}^{(l)} - \mathbf{x}_{\mathrm{N},k}^{(l)}]^2}{\sum_{k=1}^{j}[\mathbf{x}_{\mathrm{N},k}^{(l)}]^2}} \times 100\%$
PTE at the *l*-th floor*	$J_{l+4} = \frac{\max\left\lvert \mathbf{x}_{\mathrm{R},k}^{(l)} - \mathbf{x}_{\mathrm{N},k}^{(l)}\right\rvert}{\max\left\lvert \mathbf{x}_{\mathrm{N},k}^{(l)}\right\rvert} \times 100\%$

*$\mathbf{x}_{\mathrm{R}}^{(l)}$ and $\mathbf{x}_{\mathrm{N}}^{(l)}$ (l = 1, 2, 3) denote the reference displacement and the numerical displacement of the l-th floor, respectively.

Appendix 2 vRTHS evaluation criteria for the proposed delay-compensation method

Control/compensation Method	Case	Statistical algorithm	J_1 (ms)	J_2 (%)	J_3 (%)	J_4 (%)	J_5 (%)	J_6 (%)	J_7 (%)	J_8 (%)	J_9 (%)
El Centro	Case 2	Nominal	0.00	0.93	0.94	1.97	1.10	1.71	1.72	0.93	0.96
		Mean	0.08	1.09	1.21	2.25	1.48	1.94	1.95	1.10	1.12
		STD	0.13	0.20	0.22	0.57	0.39	0.68	0.68	0.46	0.46
	Case 3	Nominal	0.00	0.72	0.90	2.73	1.94	2.61	2.61	1.77	1.80
		Mean	0.04	0.80	1.03	2.78	2.02	2.63	2.63	1.78	1.80
		STD	0.08	0.10	0.23	0.81	0.64	0.93	0.93	0.69	0.69
	Case 4	Nominal	0.00	0.62	0.80	3.17	1.70	3.08	3.08	1.51	1.51
		Mean	0.04	0.81	1.11	3.27	2.13	3.06	3.07	1.69	1.69
		STD	0.08	0.15	0.29	0.91	0.51	1.01	1.01	0.60	0.60
Kobe	Case 2	Nominal	0.00	1.13	0.56	2.07	1.20	1.71	1.71	1.03	1.04
		Mean	0.06	1.32	0.84	2.36	1.44	1.90	1.90	1.14	1.14
		STD	0.09	0.23	0.30	0.56	0.30	0.78	0.78	0.46	0.46
	Case 3	Nominal	0.00	1.30	0.97	2.21	1.03	1.77	1.77	0.92	0.93
		Mean	0.04	1.35	0.94	2.22	1.19	1.75	1.75	0.95	0.95
		STD	0.08	0.11	0.16	0.42	0.32	0.66	0.65	0.44	0.44
	Case 4	Nominal	0.00	1.16	0.72	2.65	1.57	2.35	2.36	1.51	1.51
		Mean	0.07	1.26	0.77	2.94	1.73	2.63	2.63	1.61	1.61
		STD	0.13	0.17	0.18	0.92	0.56	1.11	1.11	0.62	0.62
Morgan Hill	Case 2	Nominal	0.00	1.59	1.08	2.44	1.41	1.90	1.91	1.18	1.19
		Mean	0.16	1.74	1.12	3.40	2.25	2.76	2.77	1.93	1.93
		STD	0.20	0.20	0.13	1.18	0.95	1.43	1.43	1.08	1.07
	Case 3	Nominal	0.00	1.46	0.93	2.83	1.32	2.46	2.46	1.21	1.25
		Mean	0.11	1.64	1.21	3.41	1.99	2.88	2.89	1.63	1.65
		STD	0.16	0.24	0.31	1.52	0.97	1.74	1.74	1.01	1.02
	Case 4	Nominal	0.00	1.14	0.96	3.33	2.84	3.14	3.14	2.64	2.63
		Mean	0.07	1.30	1.09	3.73	3.13	3.42	3.43	2.91	2.91
		STD	0.13	0.18	0.30	1.65	1.42	1.76	1.76	1.40	1.40